Published in final edited form as:
Cytometry A. 2010 October ; 77(10): 940–952. doi:10.1002/cyto.a.20955.

Hyperthermia Alters the Interaction of Proteins of the Mre11 Complex in Irradiated Cells

Bogdan I. Gerashchenko[1,2], **Gerirose Gooding**[1], and **Joseph R. Dynlacht**[1,3,*]

[1] Department of Radiation Oncology, Indiana University School of Medicine, Indianapolis, IN 46202, USA

[2] Department of Radiobiology and Ecology, R.E. Kavetsky Institute of Experimental Pathology, Oncology and Radiobiology, Kyiv 03022, Ukraine

[3] Department of Biochemistry and Molecular Biology, Indiana University School of Medicine, Indianapolis, IN 46202, USA

Abstract

Radiosensitization of mammalian cells by heat is believed to involve the inhibition of repair of DNA double strand breaks (DSBs). The Mre11 complex (composed of Mre11, Rad50, and Nbs1) is involved in DSB repair, and forms foci at sites of radiation-induced DSBs. Heat induces the translocation of a significant amount of Mre11, Rad50 and Nbs1 from the nucleus to the cytoplasm, but little is known about how heat affects the integrity of the proteins still remaining in nuclei, or alters kinetics of formation/disappearance of repair foci in heated, irradiated cells. Here we show that hyperthermia alters the interaction between proteins of the Mre11 complex in irradiated human melanoma cells, and inhibits the formation of repair foci. At various times after X-irradiation and/or heating (2 h at 41.5°C or 42.5°C), cells were fixed and stained for Mre11, Rad50, and Nbs1. Co-localization of proteins and formation and disappearance of nuclear foci in heated and/or irradiated cells, determined using confocal microscopy, was compared. In heated, irradiated cells, focus formation was inhibited for 2–8 h, and co-localization of the proteins of the Mre11 complex was reduced for 12–24 h post-treatment. Co-localization recovered in irradiated cells within 24 h after 41.5°C heating, but was inhibited longer after 42.5°C heating. The decreased co-localization in heated, irradiated cells suggests that there is a decrease in protein interaction, and Mre11 complexes in nuclei disassemble after heating. Such changes could be involved, at least in part, in heat-radiosensitization and inhibition of DSB repair. Also, the kinetics of disassembly and reassembly of Mre11 complexes appears to be dependent upon treatment temperature.

Keywords

DNA double-strand breaks; DNA repair foci; Mre11 complex; ionizing radiation; hyperthermia; immunofluorescence; co-localization

Introduction

Hyperthermia is currently being evaluated as a potential adjuvant to radiation therapy of cancer, since it has long been known to sensitize mammalian cells to ionizing radiation (IR)

*Corresponding author: Dr. Joseph R. Dynlacht, Address: Indiana University School of Medicine, Department of Radiation Oncology, Indiana Cancer Pavilion, RT-041, 535 Barnhill Drive, Indianapolis, IN 46202, Phone: (317) 278-3882, FAX: (317) 278-0405, jdynlach@iupui.edu.

(1,2). The molecular mechanisms for thermal radiosensitization, however, have yet to be fully delineated. Although thermal treatment of cells (40–45°C) is capable of causing transitions and structural alterations in proteins (3-5), the major challenge has been to identify those proteins whose transitions/alterations are critical in radiosensitization. Heat-radiosensitization is believed to be mediated by an inhibition of repair of IR-induced DNA double-strand breaks (DSBs) by heat (6-11). The DSB is a critical DNA lesion which can cause transformation or cell death if mis-repaired or unrestituted (12). Normally, DSBs are recognized and then repaired via two primary pathways: non-homologous DNA end-joining and homologous recombination. An absence or deficiency in either pathway results in enhanced radiosensitivity and genomic instability (13,14). The proteins of the Mre11 complex appear to play an essential role in homologous recombination in eukaryotic cells (15). Since a significant amount of each protein of the complex is initially translocated from the nucleus to the cytoplasm when cells are irradiated before heat treatments, we have speculated that the translocation of these proteins or the disassembly of the Mre11 complex may be responsible, in part, for inhibition of DSB repair and radiosensitization by hyperthermia (16,17).

Structurally, the human Mre11 complex is highly conserved. A heterotetramer of Mre11 (85 kDa) and Rad50 (153 kDa), comprised of a dimer of each protein, binds to a single Nbs1 molecule (95 kDa) (18). The Mre11-Rad50 interaction within the complex has been reported to be stable (19). The Mre11 complex, specifically Mre11 and Rad50, binds to DNA, and processes the broken ends. Nbs1 may actually serve to initiate the DNA damage-induced checkpoint response (20). Deficiency or deletion mutations in each of Mre11, Rad50, and Nbs1 genes results in hypersensitivity of cells to IR, presumably due to problems with DSB repair (21-23). The human Mre11 complex is normally uniformly distributed in the nucleus of cells. Treatment of cells with DSB-inducing agents, such as IR, results in formation of discrete and bright nuclear foci (when fluorescently stained for any of the Mre11 complex proteins), which are indicative of efficient repair of DSBs (23-28). Nuclear repair foci fluorescently stained for any of the Mre11 complex proteins or phosphorylated histone H2AX (γ-H2AX) (29) have often been used as an indicator of the DNA damage response, as their presence has been correlated with sites of DSBs.

To date, little is known about how heat affects the integrity of the Mre11 complex and alters the formation of foci in heated, irradiated cells. Here we show that heat shock alters the interaction between proteins of the Mre11 complex in unirradiated and irradiated human U-1 melanoma cells, and inhibits the induction of repair foci after irradiation. Cells were irradiated with various doses of X-rays (0–12 Gy) and then heated for 2 h at 41.5°C or 42.5°C. At various times after the treatment (0–24 h), cells were fixed/permeabilized and immunostained for Mre11, Rad50, and Nbs1. Co-localization of the proteins of the Mre11 complex and formation of Mre11/Rad50 nuclear foci in heated, irradiated cells was compared with irradiated cells that were not heated, and with heated cells that were not irradiated. Measurements of co-localization of proteins and detection/scoring of fluorescent nuclear foci were performed using confocal microscopy and intensity correlation analysis of stained proteins (28).

Materials and Methods

Cell culture, irradiation, and heat treatments

Human U-1 melanoma cells were cultured in monolayer in McCoy's 5A medium with L-glutamine (Mediatech, Herndon, VA, USA) and 10% iron-supplemented bovine calf serum (BCS; Hyclone, Logan, UT, USA). Cells were maintained at 37°C in a humidified environment of 5% CO_2 and 95% air. Forty thousand asynchronous cells were plated into each well of Lab-Tek II® 4-well tissue culture chamber slides (Nalge Nunc International,

Naperville, IL, USA) and grown for 2 days until 80–90% confluent. Five minutes prior to experiments, the culture medium in each well was replaced with 0.5 ml pre-warmed 37°C fresh medium. For samples that received only irradiation treatments, the chamber slides were placed on ice for 5 min and cells were then irradiated using a 160 kVp Faxitron X-ray machine (Wheeling, IL, USA). Cells were irradiated with doses of 0, 3, 6, or 12 Gy (dose rate: 2.44 Gy/min). The culture medium in each well was then replaced with pre-warmed 37°C fresh medium and cells were incubated for various times in a CO_2-incubator prior to fixation and immunofluorescence staining (see below). For samples that received only heat treatments, the chamber slides were placed onto a perforated rack in a 41.5°C or 42.5°C water bath for 2 h (with the slide portion immersed and the water level reaching the mid-point of the walls of the chamber slides while heating the samples). The temperature of the medium within each of the wells [as determined using a Sensortek BAT-10 thermocouple probe (Clifton, NJ)] reached the desired temperature of 41.5 or 42.5°C (± 0.1−0.2 °C) within 3 or 4.5 min, respectively after the chamber slides were placed into the water bath, after which time the medium remained steady at the desired temperature (± 0.2°C) for the duration of heating. After the heat treatment, the culture medium in each well was replaced with pre-warmed 37°C fresh medium and cells were incubated for various times in a CO_2-incubator prior to fixation and immunofluorescence staining. For samples that received both radiation and heat treatments, cells were cooled on ice for 5 min and then irradiated with doses of 0, 3, 6, or 12 Gy of X-rays. Cold medium was then replaced with pre-warmed 37°C fresh medium and cells were immediately heated for 2 h at 41.5°C or 42.5°C. The culture medium in each well was replaced with pre-warmed 37°C fresh medium and cells were incubated for various times at 37°C in a CO_2-incubator prior to preparation for immunofluorescence measurements. Samples of control cell populations were neither heated nor irradiated, but medium was changed as described above. *Changes in pH of the medium were estimated not to exceed ± 0.2 pH units at any time during the heat and radiation treatments*. Within ~ 2 h after hyperthermia treatment, most cells remained attached to the substrate. However, by 24 h post-treatment, the percentages of floating cells after heating at 42.5°C and 41.5°C was 70–80% and 20–30%, respectively. These detached cells represented the fraction of cells that were likely undergoing apoptotic death. Only attached cells were analyzed for immunostaining. The sequence of procedures for treatment and preparation of cells for immunofluorescence measurements is illustrated schematically in Figure 1.

Immunofluorescence staining

At 0, 1, 2, 4, 8, 12, or 24 h post-treatment, cells were washed twice in PBS (37°C, pH 7.4). Fixation and permeabilization of cells were performed as described (30). Briefly, cells were fixed for 10 min at room temperature in PBS containing 3% formaldehyde/2% sucrose, and then permeabilized for 5 min in Triton buffer (0.5% Triton X-100 in 20 mM HEPES, pH 7.4; 50 mM NaCl, 3 mM $MgCl_2$, 300 mM sucrose) on ice. Prior to immunofluorescence staining, cells were incubated in blocking solution (10% fetal bovine serum in PBS) for 1 h at 4°C. Cells were washed thrice with PBS and incubated overnight at 4°C with primary antibodies: anti-hRad50 mouse monoclonal antibody, dilution 1:1000 (Upstate, Lake Placid, NY, USA; clone 2C6; catalogue number: 05-525), anti-hMre11 rabbit polyclonal antibody, dilution 1:100 (Calbiochem, La Jolla, CA, USA; catalogue number: PC388), and anti-hNbs1 rabbit polyclonal antibody, dilution 1:1000 (Calbiochem, La Jolla, CA, USA; catalogue number: DR1033). Cells were then washed thrice with PBS and incubated at 37°C for 1 h with the corresponding secondary antibodies: Alexa Fluor 594 goat anti-mouse antibody, dilution 1:400 (Molecular Probes, Eugene, OR, USA; catalogue number: A11032), and Alexa Fluor 488 goat anti-rabbit antibody, dilution 1:200 (Molecular Probes; catalogue number: A11034). Since both anti-hMre11 and anti-hNbs1 antibodies were generated in rabbit, prior to staining of cells, these antibodies were used separately, but in the mixture

with anti-hRad50 (e.g., anti-hMre11 with anti-hRad50, and anti-hNbs1 with anti-hRad50). All antisera were diluted in 1% BSA in PBS. After staining, cells were washed four times with PBS, and then mounted in ProLong Gold antifade reagent (Molecular Probes, Eugene, OR, USA) followed by examination of nuclear foci. Boundaries of cell nuclei were clearly delineated under these staining conditions. DNA counterstaining with DAPI showed the same delineation of nuclear boundaries (not shown).

Laser scanning confocal microscopy

A Zeiss LSM-510Meta confocal microscope (Carl Zeiss, Jena, Germany) equipped with a C-Apochromat 63×/1.2 water immersion objective was used for examining nuclear foci. Argon (488 nm) and helium-neon (543 nm) lasers were used to excite Alexa Fluor 488 and Alexa Fluor 594, respectively. The fluorescence emitted by Alexa Fluor 488 was detected through a 505–530 nm band-pass filter. The fluorescence emitted by Alexa Fluor 594 was detected through a 560 long-pass filter. To minimize crosstalk between channels, the multi-track mode was used, which allows sequential collection of red fluorescence (from Rad50) and green fluorescence (from either Mre11 or Nbs1). Five to seven fields were randomly chosen from each sample, and from these, 2–3 representative cell nuclei were then chosen for analysis. Composite images of each nucleus were collected using LSM software (Carl Zeiss, version 4.0 SP2). These images consisted of a confocal series (z-series) of up to 18 sequential scans (0.5 μm step size). Scan speed and zoom factors were set on 6 (pixel time: 6.40 μs) and 3 *(pixel size: 0.1 μm × 0.1 μm)*, respectively. To ensure the acquisition of high quality images, the pinhole size for each channel was reduced to the extent that guaranteed a superior spatial resolution and synchronous collection of green and red fluorescence signals through the entire stack of optical sections. Green and red fluorescence signals were collected at about equally intensive gray levels. That is, amplifier and gain settings were adjusted such that green and red fluorescence intensity was nearly equal. All settings (including amplifier settings and laser power) were the same while performing the image acquisition within each set of experiments.

Co-localization analysis

Mre11/Rad50 and Nbs1/Rad50 co-localization and formation of Mre11/Rad50 nuclear foci were analyzed with the free-ware imaging software program NIH ImageJ (version 1.37c) (http://rsbweb.nih.gov/ij/)(31), modified at the Wright Cell Imaging Facility (WCIF; Toronto Western Research Institute, Canada) (available at http://www.uhnresearch.ca/wcif). Co-localization analysis was performed in accordance with instructions provided by WCIF. Briefly, background subtraction was performed on each slice of the stack of images obtained from both photomultiplier tubes (red and green fluorescence). In order to minimize noise, the images of each stack were then subjected to filtering with the “mean filter” (radius of 1 pixel). A region of interest was then defined by manually drawing the nuclear boundary on one of the images of the stack (mid-plane section of the cell). Finally, image correlation analysis was performed by combining two stacks of images (combining green and red fluorescence images). The overlap coefficient (*R*) (32) was used to quantify Mre11/Rad50 or Nbs1/Rad50 co-localization. This coefficient represents the true degree of co-localization and is not sensitive to differences in signal intensities between two channels. Its values range from 0 to 1.0, where the value of zero means no co-localization and the value of 1.0 means 100% co-localization (all pixels co-localized). The total numbers of nuclei of variously treated cells, in which Mre11/Rad50 and Nbs1/Rad50 co-localizations were examined, are shown in Tables 1 and 2,. *The Student's two-tailed t-test assuming equal variances was used for statistical analysis*.

Detection and scoring of Mre11/Rad50 nuclear foci

Mre11/Rad50 nuclear foci were analyzed as described by Gerashchenko and Dynlacht (28). Using this approach, low level fluorescence of Mre11/Rad50 foci that would normally be barely detectable upon imaging of immunofluorescence from only one protein ("hidden" foci) were enhanced using correlation analysis of fluorescence intensities from Mre11 and Rad50 proteins by combining two stacks of images (combining green and red fluorescence images). Intensity correlation analysis (ICA), developed by Li et al. (33), exists as an available option under the "co-localization analysis" menu of the WCIF ImageJ software package. The resulting combined images display positive PDM [product of the differences of the mean (33)] values reflecting the regions with best-correlated pixels. The regions with best-correlated pixels that represent foci were then quantified. In order to quantify foci, the images with positive PDM values were converted from 32-bit to 8-bit format, and then they were subjected to "connexity analysis" (found under the "3D objects counter" menu of the software package) using a 10-voxel size threshold. Positive foci, therefore, consisted of at least 11 voxels. Mre11/Rad50 foci were heterogeneous in size (0.3–2.0 μm in diameter) and all of them were included in the analysis of the average number of foci per nucleus. The average number of foci per nucleus was calculated as follows: $F = N_1/N_0$, where F is the average number of foci per nucleus; N_1 is the total number of foci; N_0 is the total number of nuclei examined. The total numbers of nuclei of cells receiving various treatments, in which Mre11/Rad50 foci were quantified, are shown in Table 3. *The Student's two-tailed t-test assuming equal variances was used for statistical analysis.*

Measurement of clonogenic survival of heated and irradiated cells

Three days prior to experiments, 2.5×10^5 cells were plated into 25 cm^2 (T-25) tissue culture flasks containing 5 ml of media and grown to a density of approximately 10^6 asynchronous cells (~ 90% confluence). Five min prior to treatment, medium in each flask was replaced with 5 ml of fresh medium. For samples that received only heat treatments, flasks containing cells were capped tightly, the necks were wrapped with parafilm, and flasks were placed in a 41.5°C or 42.5°C water bath (± 0.1 °C) for 0.5, 1, 2, 4, 6, or 15 h prior to processing for cell survival analysis. For samples that received both radiation and heat treatments, cells were cooled on ice for 5 min and then irradiated with 1.5, 3, 5, or 8 Gy while still on ice. The samples remained on ice for a total of 15 min (this included being placed on ice 5 min prior to irradiation). Cold medium was then replaced with 37°C medium and flasks were immediately capped, wrapped with parafilm, and heated in a water bath for 2 h at 41.5°C or 42.5°C. Samples which were only irradiated were processed immediately after the 15 min incubation on ice. After treatment, all samples were replaced with fresh 37°C medium and then processed. The cells were trypsinized, counted, and known numbers of cells were plated in 25 cm^2 flasks containing 5 ml medium. After about 10 days of incubation at 37°C, the cells were fixed using a 3:1 methanol to acetic acid mixture and then stained with crystal violet. The colonies were visualized with a microscope to determine surviving fraction. Any group of 50 or more cells was considered a colony.

Results

Heat-induced Cell Killing and Heat-radiosensitization

Figure 2A shows clonogenic cell survival curves for human U-1 melanoma cells that were heated at 41.1°C or 42.5°C for up to 15 h. Heating at 42.5°C was much more cytotoxic than heating at 41.5°C. The difference in cytotoxicity between the two temperatures is evident after one hour of heating. While a plateau is reached for the 41.5°C survival curve, the surviving fraction of 42.5°C-heated cells continued to decline with increasing duration of heating.

Heating for 2 h at 42.5°C resulted in a surviving fraction that was 10-fold less than the surviving fraction of 41.5°C-heated cells. Since these two heat treatments produced significant differences in heat cytotoxicity, we chose to compare these treatments in our studies of the Mre11 complex in heated or heated and irradiated cells.

Survival curves for cells exposed to various doses of X-rays or cells which were irradiated prior to being heated for 2 h at 41.5°C or 42.5°C are shown in Figures 2B and 2C. A 3 Gy dose of radiation (alone) reduced the surviving fraction by 50%, while the surviving fraction after irradiation with 6 Gy was approximately 0.1 (the surviving fraction after irradiation with 12 Gy was estimated to be less than 0.01). Both thermal treatments of irradiated cells caused significant radiosensitization when surviving fractions were normalized for cytotoxicity from the respective heat treatments (Fig. 2B and 2C). The amount of radiosensitization for both heat treatments was similar for cells irradiated with up to 5 Gy; however, heating at 42.5°C appeared to result in ~ 5-fold more radiosensitization than the 41.5°C treatment in cells irradiated with 8 Gy (Fig. 2B vs. 2C).

Hyperthermia inhibits the formation of Mre11/Rad50 nuclear foci in irradiated cells

Figure 3 shows the kinetics of Mre11/Rad50 focus formation in heated, irradiated cells and in cells that were either only irradiated with 3–12 Gy or heated at 42.5°C or 41.5°C. In cells that were only irradiated, the dynamics of focus formation depended upon the magnitude of the radiation dose. The average number of foci per nucleus (*F*) in 3 Gy-irradiated cells reached a maximum level (~ 8 foci per nucleus) at 2 h post-irradiation (Fig. 3A), while *F* values for 6 Gy-and 12 Gy-irradiated cells reached a maximum level (12–14 and 10–12 foci per nucleus, respectively) within 4–8 h post-irradiation (Fig. 3B-D). Radiation dose appeared to correlate with persistence of Mre11/Rad50 foci. The average numbers of foci per nucleus in irradiated cells declined with time in a dose-dependent manner. For example, at 24 h post-irradiation, the *F* value of 3 Gy-irradiated cells was ~ 2 foci per nucleus (same as for unirradiated control cells; Fig. 3A), while *F* values of 6 Gy- and 12 Gy-irradiated cells were ~ 5, and 9–10 foci per nucleus, respectively (Fig. 3B-D). At 48 h post-irradiation, the *F* value of 12 Gy-irradiated cells was much lower than that at 24 h post-irradiation (~ 5 foci per nucleus; Fig. 3C). For cells that were only heated (heated for 2 h at 41.5°C or at 42.5°C), *F* values (~ up to 12 h) were similar to *F* values of unheated, unirradiated control cells (1–3 foci per nucleus; Fig. 3A-D). There was only a slight elevation of *F* values of these cells at 12–24 h post-treatment (up to 3–4 foci per nucleus; Fig. 3A-D). Irradiated cells (3 Gy, 6 Gy, and 12 Gy) that were heated at 42.5°C for 2 h showed no increase of focus formation up to 8 h post-treatment (1–3 foci per nucleus; Fig. 3A-C). An increase of focus formation in these cells occurred only at 12–24 h post-treatment (4–7 foci per nucleus; Fig. 3A-C). At 12 and 24 h post-treatment, *F* values of 42.5°C-heated 6 Gy- and 12 Gy-irradiated cells significantly differed from *F* values of cells that were only heated ($P < 0.05$; Fig. 3B and 3C), while at these times post-treatment, *F* values of 42.5°C-heated 3 Gy-irradiated cells were similar to *F* values of cells that were only heated ($P > 0.05$; Fig. 3A). Although at 24 h post-treatment, 42.5°C-heated, 12 Gy-irradiated cells showed an increase of focus formation (up to ~ 7 foci per nucleus, compared to ~ 4 foci per nucleus at 12 h post-treatment), the number of foci in these cells decreased to ~ 3 foci per nucleus at 48 h post-treatment (Fig. 3C). In contrast to 42.5°C-heated, 12 Gy-irradiated cells that showed no increase of focus formation up to 8 h post-treatment, 41.5°C-heated, 12 Gy-irradiated cells showed no increase in focus formation only through the first 2 h post-treatment (compare Fig. 3C with 3D). From 4 to 12 h post-treatment, there was an increase in focus formation in these cells (~ 5 foci per nucleus). Interestingly, at 24 h post-treatment, the *F* value of 41.5°C-heated, 12 Gy-irradiated cells was ~ 9 foci per nucleus (Fig. 3D). However, at this same time post-treatment (24 h), the *F* value of 42.5°C-heated, 12 Gy-irradiated cells was ~ 7 foci per nucleus (Fig. 3C).

Hyperthermia affects Mre11/Rad50 and Nbs1/Rad50 nuclear co-localization in irradiated cells

Figure 4 shows the kinetics of changes in Mre11/Rad50 and Nbs1/Rad50 nuclear co-localization of cells that were only irradiated with 3-12 Gy, heated at 41.5°C or 42.5°C, or cells which were heated and irradiated. In general, 3 Gy-, 6 Gy-, and 12 Gy-irradiated cells did not show significant differences in Mre11/Rad50 co-localization for up to 24 h post-irradiation compared to unirradiated control cells. However, when compared to irradiated cells, there were significant changes in Mre11/Rad50 co-localization of cells that were heated for 2 h at either 41.5°C or 42.5°C, and cells that were irradiated (3 Gy, 6 Gy, and 12 Gy) and then heated and incubated at 37° C for up to 24 h after treatment (Fig. 4A-D). Cells that were only heated at 42.5°C and cells that were irradiated (3 Gy, 6 Gy, or 12 Gy) and then heated at 42.5°C showed similar patterns of Mre11/Rad50 co-localization (Fig. 4A-C). These cells showed a gradual reduction in Mre11/Rad50 co-localization up to 8 h post-treatment. By 12 h post-treatment, cells began to show an increase in Mre11/Rad50 co-localization, nearly reaching the *R* values exhibited by control cells. It should be noted that 42.5°C-heated, irradiated cells, similar to cells that were only irradiated, did not show any radiation dose-dependent changes in Mre11/Rad50 co-localization (Fig. 4A-C). Using unheated, unirradiated control cells as a reference, compared to cells which were only heated at 42.5°C and heated at 42.5°C after irradiation with 12 Gy, cells heated at 41.5°C or heated at 41.5°C after irradiation with 12 Gy showed a drastic decrease in Mre11/Rad50 co-localization at 0-1 h post-treatment (Fig. 4C vs. 4D). Moreover, unlike 42.5°C-heated unirradiated and 42.5°C-heated 12 Gy-irradiated cells that showed a decrease and then an increase in Mre11/Rad50 co-localization, 41.5°C-heated unirradiated and 41.5°C-heated 12 Gy-irradiated cells exhibited two distinct cycles of recovery of Mre11/Rad50 co-localization (Fig. 4C vs. 4D) [at 8 and 24 h post-treatment in unirradiated heated cells, and at 4 and 24 h in cells that were heated at 41.5°C after 12 Gy-irradiation (Fig. 4D)]. The *R* value of the first increase in Mre11/Rad50 co-localization of 41.5°C-heated, 12 Gy-irradiated cells was very close to the *R* value obtained for unheated, unirradiated control cells ($R \sim 0.9$), while the *R* value of the second increase in Mre11/Rad50 co-localization of these cells ($R \sim 0.92$) was significantly higher than the *R* value exhibited by control cells ($P < 0.05$; Fig. 4D).

Similar to Mre11/Rad50 co-localization, Nbs1/Rad50 co-localization after irradiation was not dose-dependent, and in general, co-localization was not much different when observed for up to 24 h post-irradiation compared to unirradiated control cells (Fig. 4A-D). Compared to Mre11/Rad50 co-localization in 42.5°C-heated unirradiated cells and cells heated at 42.5°C and irradiated with 3–12 Gy at 0 h post-treatment, there was a significant drop in Nbs1/Rad50 co-localization in these cells (indicated by arrows; Fig. 4A-C). The decrease of co-localization of Nbs1/Rad50 in 42.5°C-heated unirradiated cells and cells heated at 42.5°C and irradiated with 3–12 Gy continued for up to 24 h post-treatment (Fig. 4A-C). Although there were some fluctuations in Nbs1/Rad50 co-localization of these heated unirradiated and heated irradiated cells for up to 24 h post-treatment, *R* values were considerably lower than *R* values exhibited by control cells (Fig. 4A-C). In 42.5°C-heated cells irradiated with 3–12 Gy as well, the changes in Nbs1/Rad50 co-localization were not radiation dose-dependent (Fig. 4A-C). Like Mre11/Rad50 co-localization, the changes in Nbs1/Rad50 co-localization of 41.5°C-heated unirradiated and 41.5°C-heated 12 Gy-irradiated cells considerably differed from the changes in Nbs1/Rad50 co-localization of 42.5°C-heated unirradiated and 42.5°C-heated 12 Gy-irradiated cells (Fig. 4D vs. Fig. 4A, 4B, and 4C). Using unheated unirradiated control cells as a reference, compared to unirradiated cells that were heated at 42.5°C, unirradiated cells that were heated at 41.5°C showed no significant differences in Nbs1/Rad50 co-localization at 0 h post-treatment ($P > 0.05$; Fig. 4D vs. 4A, 4B, and 4C). In addition, these cells showed two apparent recovery periods (8 and 24 h post-treatment) in Nbs1/Rad50 co-localization with an *R* value of ~ 0.87; this was not significantly different (*P*

> 0.05) than the *R* value for control cells (*R* ~ 0.88; Fig. 4D). In contrast to 41.5°C-heated unirradiated cells, 41.5°C-heated 12 Gy-irradiated cells showed a significant reduction in Nbs1/Rad50 co-localization at 0 h post-treatment compared to control cells ($P < 0.05$), and recovery of Nbs1/Rad50 co-localization occurred within 24 h post-treatment, with an *R* value of ~ 0.88 (almost the same as in control cells)(Fig. 4D). In general, immediately after treatment, the changes in Nbs1/Rad50 co-localization of 41.5°C-heated unirradiated and 41.5°C-heated 12 Gy-irradiated cells were similar to the changes in Mre11/Rad50 co-localization (Fig. 4D).

In order to assess the pattern of Mre11/Rad50 or Nbs1/Rad50 nuclear co-localization in cells after irradiation, hyperthermia treatments, or the combination of radiation and hyperthermia treatments, ICA-generated stacks of confocal images of co-localized proteins in the nuclei of 12 Gy-irradiated, 42.5°C-heated unirradiated, 42.5°C-heated 12 Gy-irradiated, and unheated unirradiated (control) cells at 0 and 4 h post-treatment were compared. Representative ICA-generated middle plane confocal images of co-localized Mre11/Rad50 and Nbs1/Rad50 proteins in cells receiving the various aforementioned treatments are shown in Figures 5 and 6, respectively. At 0 h post-irradiation, the nuclei of 12 Gy-irradiated cells showed no changes in the pattern of Mre11/Rad50 co-localization, compared to the nuclei of control cells (Fig. 5A vs. 5B). Control cells as well as 12 Gy-irradiated cells at 0 h post-irradiation showed a low granularity in the texture of co-localized proteins in their nuclei (Fig. 5A and 5B, respectively). Due to this peculiarity, the nuclear boundaries in these cells looked more distinct and smooth. Granularity was different, however, in heated or heated and irradiated cells. Cells that were only heated or cells that were irradiated and then heated showed a similar pattern of Mre11/Rad50 nuclear co-localization at 0 h post-treatment, but displayed an increase of granularity in the texture of co-localized proteins (Fig. 5D and 5E, respectively). The nuclear boundaries of these cells looked less distinct and smooth. It should also be noted that in these cells, co-localized proteins were distributed less uniformly throughout the nuclei, compared to control or 12 Gy-irradiated cells. The nuclei of 12 Gy-irradiated cells at 4 h post-irradiation clearly showed the IR-induced Mre11/Rad50 foci (Fig. 5C). The background Mre11/Rad50 staining of nuclei of these cells was also noticeably reduced. Cells that were irradiated and then heated revealed a few very small foci per nucleus at 4 h post-treatment (Fig. 5F). The nuclei of these cells, compared to the nuclei of 42.5°C-heated 12 Gy-irradiated cells fixed immediately (0 h) post-treatment, showed reduced amounts of co-localized proteins (Fig. 5F vs. 5E). The pattern of Mre11/Rad50 co-localization in the nuclei of 42.5°C-heated unirradiated cells at 4 h post-treatment (image not shown) was similar to that of the nuclei of 42.5°C-heated 12 Gy-irradiated cells at 4 h post-treatment (Fig. 5F).

As observed with Mre11/Rad50 co-localization, Nbs1/Rad50 co-localization was unchanged in 12 Gy-irradiated cells immediately after treatment compared to control cells (Fig. 6A vs. 6B). As with Mre11/Rad50 foci, Nbs1/Rad50 foci were clearly observed in the nuclei of 12 Gy-irradiated cells at 4 h post-irradiation (Fig. 6C). However, unlike Mre11/Rad50 co-localization in the nuclei of 42.5°C-heated unirradiated and 42.5°C-heated 12 Gy-irradiated cells at 0 h post-treatment, Nbs1/Rad50 co-localization in the nuclei of these cells decreased significantly (Fig. 6D and 6E, respectively). Also, co-localized Nbs1 and Rad50 were much less uniformly distributed throughout the nuclei of these cells, compared to control cells or 12 Gy-irradiated cells at 0 h post-irradiation (Fig. 6D and 6E vs. 6A or 6D). The pattern of Nbs1/Rad50 nuclear co-localization in 42.5°C-heated 12 Gy-irradiated cells at 4 h post-treatment was similar to that in 42.5°C-heated unirradiated or 42.5°C-heated 12 Gy-irradiated cells at 0 h post-treatment (Fig. 6F vs. 6D or 6E). There was a lack of nuclear foci in these cells compared to unheated 12 Gy-irradiated cells at 4 h post-irradiation (Fig. 6F vs. 6C). The pattern of Nbs1/Rad50 co-localization of the nuclei of 42.5°C-heated unirradiated cells at 4 h post-treatment (image not shown) was similar to that of the nuclei of 42.5°C-

heated 12 Gy-irradiated cells at 4 h post-treatment (Fig. 6F). Mid-plane confocal images of Nbs1 (green), Rad50 (red), and merged Nbs1 (green) and Rad50 (red) immunofluorescence in the nucleus of one of the 42.5°C-heated unirradiated cells at 0 h post-treatment are shown in Figure 7A, B, and C, respectively. It should be noted that a significant portion of Nbs1 was seen in the cytoplasm, while cytoplasmic content of Rad50 was extremely low.

Discussion

The formation of foci containing various DNA repair proteins appears to be a prerequisite for repair of radiation-induced DNA damage. Our results indicate that hyperthermia (41.5°C or 42.5°C for 2 h) significantly inhibited Mre11/Rad50 focus formation in the nuclei of irradiated cells (Fig. 3A-D), and the magnitude of this inhibition was temperature-dependent (Fig. 3C vs. 3D). Although, there was a recovery of focus formation in heated, irradiated cells with increasing time post-treatment, the maximal *F* values of these cells during the period of observation were not as great as the maximal *F* values of cells that were only irradiated. Based on our finding that the number of nuclear foci in cells that had been incubated at 37°C for 24 h after being irradiated with 3 Gy-, 6 Gy-, or 12 Gy and heated at 42.5°C was increased up to ~ 4, 5, and 7 foci per nucleus respectively (Fig. 3A-C), it is possible that the repair of DSBs in these heated, irradiated cells is dependent upon the magnitude of the radiation dose. In cells that are irradiated but not heated, DSB repair is dose-dependent (34,35). However, for cells that were only irradiated, a 12-Gy exposure did not result in an enhanced number of nuclear foci being formed, when compared to cells that received a 6-Gy exposure (Fig. 3B vs. 3C or 3D). This finding, while in agreement with recently published data (28), is perplexing since IR induces DSBs in a dose-dependent linear fashion at the doses under consideration (34,35). The discrepancy could be due to a "saturation effect," whereby the number of foci per nucleus remains unchanged or nearly so, despite progressive induction of DSBs with increasing dose. Indeed, at 8 h post-irradiation, the maximal *F* value of 12 Gy-irradiated cells was slightly lower than the maximal *F* value of 6 Gy-irradiated cells (Fig. 3B vs. 3C or 3D). Since nuclear foci are believed to be indicators of DSBs and we noted a temperature-dependent inhibition of radiation-induced nuclear foci [heating of cells at 42.5°C compared to heating of cells at 41.5°C (Fig. 3C vs. 3D)], it is attractive to speculate that heat dose-dependent inhibition of formation of Mre11 foci may would result in a heat dose-dependent inhibition of repair of radiation-induced DSBs. This assumption is supported by findings that show that the rate of repair of DSBs and single strand breaks is increased in irradiated cells heated at temperatures less than 42°C (1,36,37) but is decreased in irradiated cells heated at temperatures greater 42°C, ultimately leading to increased frequency of misrepair (6–9,11). Since heat radiosensitization is believed to be mediated by the inhibition of rejoining of IR-induced DSBs, it does not seem surprising that with higher doses of radiation (e.g., 8 Gy), 42.5°C hyperthermia resulted in much more radiosensitization of cells than 41.5°C hyperthermia (Fig. 2B vs. 2C).

Mre11/Rad50 focus formation in cells that were only irradiated was accompanied by insignificant fluctuations in either Mre11/Rad50 or Nbs1/Rad50 co-localization, suggesting there was no change in the integrity of Mre11 complexes of irradiated cells (Fig. 4A-D). A significant drop in Nbs1/Rad50 co-localization, compared to Mre11/Rad50 co-localization, in 42.5°C-heated cells irradiated with 3, 6, and 12 Gy, and 42.5°C-heated unirradiated cells observed 0–1 h post-treatment (Fig. 4A-C) can be explained by a reduced binding of Nbs1 to Mre11-Rad50 sub-complexes, which are likely to form aggregates in these cells (an increase of granularity in the texture of co-localized Mre11 and Rad50; Fig. 5D and 5E). The rapid and significant drop we observed in Nbs1/Rad50 co-localization, when taken together with the decreasing *R* values (≤ 0.86) for cells through up to 24 h post-treatment, indicates that Nbs1 may be more susceptible to 42.5°C-induced structural changes than Mre11 and/or Rad50 in both heated, irradiated cells and cells that were only heated (Fig.

4A-C). In contrast to Nbs1/Rad50 co-localization, Mre11/Rad50 co-localization in these cells gradually decreased and then increased (Fig. 4A-C), suggesting disaggregation/dissociation of Mre11-Rad50 sub-complexes (up to 8–12 h post-treatment) and subsequent recovery of complex structure and intranuclear localization (up to 24 h post-treatment). A partial disaggregation of intranuclear proteins that were unfolded and aggregated due to heat shock has been reported (38,39). The significant drop in Mre11/Rad50 co-localization in 41.5°C-heated 12 Gy-irradiated cells, compared to Mre11/Rad50 co-localization in 42.5°C-heated 12 Gy-irradiated cells, at 0 h post-treatment (Fig. 4D vs. 4C), can be explained as follows. When the Mre11 complexes re-locate from the sites of their primary localization to the sites of IR-induced DSBs, heating at 41.5°C, in contrast to heating at 42.5°C, may cause dissociation of Mre11-Rad50 sub-complexes with little or no aggregation. The possibility of prompt dissociation of Mre11 complexes during and/or immediately after heating of irradiated cells was further confirmed by a considerable drop in Nbs1/Rad50 co-localization in 41.5°C-heated 12 Gy-irradiated cells at 0 h post-treatment (Fig. 4D). At this time post-treatment, there was an insignificant drop in Nbs1/Rad50 co-localization in 41.5°C-heated unirradiated cells, compared to Nbs1/Rad50 co-localization in 42.5°C-heated unirradiated cells (Fig. 4D vs. Fig. 4A-C); an interpretation for this observation may be that there are less alterations in the binding of Nbs1 to Mre11-Rad50 sub-complexes in 41.5°C-heated unirradiated cells than in 42.5°C-heated unirradiated cells (due to fewer structural alterations in these proteins caused by heating at the lower temperature). As a result of fewer, or potentially reversible, structural alterations in Mre11 complex proteins after heating of unirradiated and irradiated cells at 41.5°C, there were dynamic changes in both Mre11/Rad50 and Nbs1/Rad50 co-localization in these cells: there were two nearly concordant increases in co-localization of these proteins observed after 2 h post-treatment, suggesting dynamism of intermolecular interactions (Fig. 4D). The initial increase in Mre/Rad50 and Nbs1/Rad50 co-localization of 41.5°C-heated unirradiated and 41.5°C-heated 12 Gy irradiated cells within 4–8 h post-treatment is probably due to active re-assembly of Mre11 complexes (Fig. 4D). Subsequent “peaks and valleys” in Mre/Rad50 and Nbs1/Rad50 co-localization in these cells within 8–24 h post-treatment (Fig. 4D) may be due to redistribution and accumulation of Mre11 complexes to the primary sites of their localization (predominantly in cells that were only heated) or to the sites of IR-induced DSBs (predominantly in cells that were irradiated and then heated). The observation that at 24 h post-treatment, 41.5°C-heated 12 Gy-irradiated cells showed even more of an increase in both Mre11/Rad50 and Nbs1/Rad50 co-localizations compared to 41.5°C-heated unirradiated cells ($P < 0.05$), is likely to be indicative of an active DSB repair process, which requires all three proteins of the Mre11 complex to be functional (Fig. 4D). This finding is supported by our focus formation data that show that these cells at 24 h post-treatment had a significant increase in the number of foci per nucleus (up to ~ 9 foci per nucleus; Fig. 3D).

From our co-localization data, one can assume that heating of unirradiated or irradiated cells at 42.5°C for 2 h can cause alterations in Mre11 complex proteins to a considerably greater degree than heating at 41.5°C for 2 h. This assumption seems reasonable in light of the finding that the more severe heat treatment resulted in 10-fold less cell survival (Fig. 2A).

A rapid decrease of Nbs1/Rad50 co-localization within the nuclei (Fig. 4A-C; Fig. 6D and 6E) accompanied by the appearance of Nbs1-containing aggregates in the extranuclear area (Fig. 7), particularly after heating of unirradiated and irradiated cells at 42.5°C, suggests that Nbs1 can readily dissociate from the complex with Mre11 and Rad50 and delocalize after heat shock. Nbs1 together with Mre11 and Rad50 has been found to reversibly translocate from the nucleus to the cytoplasm in U-1 melanoma cells after 42.5–45.5°C heating, while levels of each protein remain unchanged (16,17,40). Nbs1 has been found to translocate to a greater degree than Mre11 and Rad50 (16,17,40). This could be a reason why Nbs1

immunofluorescence in the cytoplasm of heated cells was increased compared to Rad50 (Fig. 7). Heat-induced formation of aggregates of Mre11 and Rad50 (Fig. 5D and 5E) is likely to prevent their rapid translocation from the nucleus. Dynlacht and co-workers (16,17,40) have also reported an increase in translocation of all three proteins in irradiated cells (12 Gy) that were heated at 42.5–45.5°C, which, in part, may be responsible for heat radiosensitization. Although this finding cannot be confirmed from our co-localization data presented in this report, it should be noted that heating at 41.5°C resulted in a greater reduction of Mre11/Rad50 and Nbs1/Rad50 nuclear co-localization in 12 Gy-irradiated cells than in 41.5°C-heated unirradiated cells, within 0–1 h post-treatment (Fig. 4D).

It is likely that there is less protein aggregation in 41.5°C-heated cells than in 42.5°C-heated cells. Thus, one can assume that the proteins of the Mre11 complex (mainly Mre11 and Rad50) can more readily redistribute at 41.5°C than at 42.5°C. An increase of Mre11 in the cytoplasm accompanied by its concomitant decrease in the nuclei has been observed immediately after heating of heat-resistant human adenocarcinoma cells at 41.1°C (41). Xu at al. (41) have also reported that 41.1°C hyperthermia may alter the interaction of Rad50 with other proteins of the complex (a reduction in the amount of Rad50 that was associated with Mre11 when total cellular lysates were analyzed). Thus, temperature-dependent aggregation/disaggregation of the Mre11 complex proteins (specifically Mre11 and Rad50) may dictate the extent of their translocation from the nucleus to the cytoplasm. Even though treatment of cells at 41.5° C for 2 h is less severe than heating at *42.5°C* for 2 h, these proteins may still undergo conformational changes, although it seems less likely that they would aggregate while relocating to the sites of DSBs.

Heat-induced conformational changes (unfolding, aggregation, etc.) in nuclear proteins are believed to be critical for heat-radiosensitization (39,42,43), but specific proteins involved in heat-radiosensitization have yet to be identified. Our data suggest that heating alone is sufficient to induce alterations in co-localization of proteins of the Mre11 complex (as evidenced by changes observed in heated or heated irradiated cells immediately after treatment). Since the Mre11 complex is crucial for repairing DSBs, heat-induced structural alterations in the proteins composing this complex may be responsible for heat-radiosensitization.

We propose that a reduction in co-localization of proteins of the Mre11 complex and inhibition of Mre11/Rad50 focus formation in heated, irradiated cells is likely to be due to heat-induced conformational changes in all three proteins of the Mre11 complex, and that this may eventually lead to disassembly of the Mre11 complex. The complex may be re-assembled, but the kinetics of reassembly is dependent upon the heat dose. Our data also suggest that Nbs1 is likely to be more susceptible to structural changes with increasing temperature, compared to the two other proteins of the complex (Mre11 and Rad50), which normally form a stable association. Thus, it is attractive to speculate that heat-induced conformational changes that reduce the association between all three proteins of the complex may be responsible for heat-radiosensitization and inhibition of DSB repair.

Acknowledgments

This work was supported by NIH grant CA108582 (JRD). The authors thank Jennifer Lopez and Joy Garrett for technical assistance, and wish to acknowledge support from the Indiana Center for Biological Microscopy, at which the confocal microscopy work was performed.

Literature Cited

1. Ben-Hur E, Elkind MM, Bronk BV. Thermally enhanced radioresponse of cultured Chinese hamster cells: inhibition of repair of sublethal damage and enhancement of lethal damage. Radiat Res. 1974; 58:38–51. [PubMed: 10876605]
2. Dewey WC, Hopwood LE, Sapareto LA, Gerweck LE. Cellular responses to combinations of hyperthermia and radiation. Radiology. 1977; 123:463–474. [PubMed: 322205]
3. Lepock JR, Cheng KH, Al-Qysi H, Kruuv J. Thermotropic lipid and protein transitions in Chinese hamster lung cell membranes: relationship to hyperthermic cell killing. Can J Biochem. 1983; 61:421–427.
4. Lepock JR, Frey HE, Rodahl AM, Kruuv J. Thermal analysis of CHL V79 cells using differential scanning calorimetry: implications for hyperthermic cell killing and the heat shock response. J Cell Physiol. 1988; 137:14–24. [PubMed: 3170654]
5. Freeman ML, Borrelli MJ, Meredith MJ, Lepock JR. On the path to the heat shock response: destabilization and formation of partially folded protein intermediates, a consequence of protein thiol modification. Free Radic Biol Med. 1999; 26:737–745. [PubMed: 10218664]
6. Corry PM, Robinson S, Getz S. Hyperthermic effects on DNA repair mechanisms. Radiology. 1977; 123:475–482. [PubMed: 847220]
7. Dewey WC, Sapareto SA, Betten DA. Hyperthermic radiosensitization of synchronous Chinese hamster cells: relationship between lethality and chromosomal aberrations. Radiat Res. 1978; 76:48–59. [PubMed: 569879]
8. Mills MD, Meyn RE. Effects of hyperthermia on DNA repair mechanisms. Radiat Res. 1981; 87:314–328. [PubMed: 7267998]
9. Radford IR. Effects of hyperthermia on the repair of X-ray induced DNA double strand breaks in mouse L cells. Int J Radiat Biol. 1983; 5:551–557.
10. Dikomey E, Franzke J. Effect of heat on induction and repair of DNA strand breaks in X-irradiated CHO cells. Int J Radiat Biol. 1992; 61:221–233. [PubMed: 1351910]
11. Wong RSL, Dynlacht J, Cedervall B, Dewey WC. Analysis by pulsed field gel electrophoresis of DNA double-strand breaks induced by heat and/or X-irradiation in bulk and replicating DNA of CHO cells. Int J Radiat Biol. 1995; 68:141–152. [PubMed: 7658139]
12. Khanna KK, Jackson SP. DNA double-strand breaks: signaling, repair and the cancer connection. Nat Genet. 2001; 27:247–254. [PubMed: 11242102]
13. Thompson LH, Schild D. Recombinational DNA repair and human disease. Mutat Res. 2002; 509:49–78. [PubMed: 12427531]
14. Kampinga HH, Dynlacht JR, Dikomey E. Mechanism of radiosensitization by hyperthermia (≥ 43°C) as derived from studies with DNA repair defective mutant cell lines. Int J Hyperthermia. 2004; 20:131–139. [PubMed: 15195507]
15. Tauchi H, Kobayashi J, Morishima K, van Gent DC, Shiraishi T, Verkaik NS, vanHeems D, Ito E, Nakamura A, Sonoda E, et al. Nbs1 is essential for DNA repair by homologous recombination in higher vertebrate cells. Nature. 2002; 420:93–98. [PubMed: 12422221]
16. Zhu WG, Seno J, Beck BD, Dynlacht JR. Translocation of Mre11 from the nucleus to the cytoplasm as a mechanism of radiosensitization by heat. Radiat Res. 2001; 156:92–102.
17. Seno DJ, Dynlacht JR. Intracellular redistribution and modification of proteins of the Mre11/Rad50/Nbs1 DNA repair complex following irradiation and heat-shock. J Cell Physiol. 2004; 199:157–170. [PubMed: 15039997]
18. Williams RS, Williams JS, Tainer JA. Mre11-Rad50-Nbs1 is a keystone complex connecting DNA repair machinery, double-strand break signaling, and the chromatin template. Biochem Cell Biol. 2007; 85:509–520. [PubMed: 17713585]
19. Dolganov GM, Maser RS, Novikov A, Tosto L, Chong S, Bressan DA, Petrini JHJ. Human Rad50 is physically associated with human Mre11: identification of a conserved multiprotein complex implicated in recombinational DNA repair. Mol Cell Biol. 1996; 16:4832–4841. [PubMed: 8756642]

20. Lee JH, Ghirlando R, Bhaskara V, Hoffmeyer MR, Gu J, Paull TT. Regulation of Mre11/Rad50 by Nbs1: effects on nucleotide-dependent DNA binding and association with ataxia-telangiectasia-like disorder mutant complexes. J Biol Chem. 2003; 278:45171–45181. [PubMed: 12966088]
21. Luo G, Yao MS, Bender CF, Mills M, Bladl AR, Bradley A, Petrini JHJ. Disruption of *mRad50* causes embryonic stem cell lethality, abnormal embryonic development, and sensitivity to ionizing radiation. Proc Natl Acad Sci USA. 1999; 96:7376–7381. [PubMed: 10377422]
22. Yamaguchi-Iwai Y, Sonoda E, Sasaki MS, Morrison C, Haraguchi T, Hiraoka Y, Yamashita YM, Yagi T, Takata M, Price C, et al. Mre11 is essential for the maintenance of chromosomal DNA in vertebrate cells. EMBO J. 1999; 18:6619–6629. [PubMed: 10581236]
23. Desai-Mehta A, Cerosaletti KM, Concannon P. Distinct functional domains of nibrin mediate Mre11 binding, focus formation, and nuclear localization. Mol Cell Biol. 2001; 21:2184–2191. [PubMed: 11238951]
24. Maser RS, Monsen KJ, Nelms BE, Petrini JHJ. hMre11 and hRad50 nuclear foci are induced during the normal cellular response to DNA double-strand breaks. Mol Cell Biol. 1997; 17:6087–6096. [PubMed: 9315668]
25. Carney JP, Maser RS, Olivares H, Davis EM, Le Beau M, Yates JR 3rd, Hays L, Morgan WF, Petrini JHJ. The hMre11/hRad50 protein complex and Nijmegen breakage syndrome: linkage of double-strand break repair to the cellular DNA damage response. Cell. 1998; 93:477–486. [PubMed: 9590181]
26. Digweed M, Demuth I, Rothe S, Scholz R, Jordan A, Grötzinger C, Schindler D, Grompe M, Sperling K. SV40 large T-antigen disturbs the formation of nuclear DNA-repair foci containing MRE11. Oncogene. 2002; 21:4873–4878. [PubMed: 12118365]
27. van Veelen LR, Cervelli T, van de Rakt MWMM, Theil AF, Essers J, Kanaar R. Analysis of ionizing radiation-induced foci of DNA damage repair proteins. Mutat Res. 2005; 574:22–33. [PubMed: 15914204]
28. Gerashchenko BI, Dynlacht JR. A tool for enhancement and scoring of DNA repair foci. Cytometry A. 2009; 75A:245–252. [PubMed: 18836995]
29. Sedelnikova OA, Rogakou EP, Panyutin IG, Bonner WM. Quantitative detection of ^{125}IdU-induced DNA double-strand breaks with γ-H2AX antibody. Radiat Res. 2002; 158:486–492. [PubMed: 12236816]
30. Scully R, Chen J, Ochs RL, Keegan K, Hoekstra M, Feunteun J, Livingston DM. Dynamic changes of BRCA1 subnuclear location and phosphorylation state are initiated by DNA damage. Cell. 1997; 90:425–435. [PubMed: 9267023]
31. Rasband, WS. Bethesda, Maryland: U.S. National Institute of Health; 1997–2007. ImageJ. Available at: http://rsb.info.nih.gov/ij/
32. Manders EMM, Verbeek FJ, Aten JA. Measurement of co-localization of objects in dual-colour confocal images. J Microsc. 1993; 169:375–382.
33. Li Q, Lau A, Morris TJ, Guo L, Fordyce CB, Stanley EF. A syntaxin 1, Gα_0, and N-type calcium channel complex at a presynaptic nerve terminal: analysis by quantitative immunocolocalization. J Neurosci. 2004; 24:4070–4081. [PubMed: 15102922]
34. Nevaldine B, Longo JA, King GA, Vilenchik M, Sagerman RH, Hahn PJ. Induction and repair of DNA double-strand breaks. Radiat Res. 1993; 133:370–374. [PubMed: 8451389]
35. Löbrich M, Rydberg B, Cooper PK. Repair of X-ray-induced DNA double-strand breaks in specific *Not* I restriction fragments in human fibroblasts: joining of correct and incorrect ends. Proc Natl Acad Sci U S A. 1995; 92:12050–12054. [PubMed: 8618842]
36. Dikomey E. Effect of hyperthermia at 42 and 45°C on repair of radiation induced DNA strand breaks in CHO cells. Int J Radiat Biol Relat Stud Phys Chem Med. 1982; 41:603–614. [PubMed: 6981617]
37. Warters RL, Axtell J. Repair of DNA strand breaks at hyperthermic temperatures in Chinese hamster ovary cells. Int J Radiat Biol. 1992; 61:43–48. [PubMed: 1345930]
38. Stege GJJ, Li GC, Li L, Kampinga HH, Konings AW. On the role of hsp72 in heat-induced intranuclear protein aggregation. Int J Hyperthermia. 1994; 10:659–674. [PubMed: 7806923]
39. Stege GJJ, Kampinga HH, Konings AW. Heat-induced intranuclear protein aggregation and thermal radiosensitization. Int J Radiat Biol. 1995; 67:203–209. [PubMed: 7884289]

40. Dynlacht JR, Xu M, Pandita RK, Wetzel EA, Roti Roti JL. Effects of heat shock on the Mre11/Rad50/Nbs1 complex in irradiated or unirradiated cells. Int J Hyperthermia. 2004; 20:144–156. [PubMed: 15195509]

41. Xu M, Myerson RJ, Straube WL, Moros EG, Lagroye I, Wang LL, Lee JT, Roti Roti JL. Radiosensitization of heat resistant human tumour cells by 1 hour at 41.1°C and its effect on DNA repair. Int J Hyperthermia. 2002; 18:385–403. [PubMed: 12227926]

42. Beck BD, Dynlacht JR. Heat-induced aggregation of XRCC5 (Ku80) in non-tolerant and thermotolerant cells. Radiat Res. 2001; 156:767–774. [PubMed: 11741501]

43. Laszlo A, Davidson T, Harvey A, Sim JE, Malyapa RS, Spitz DR, Roti Roti JL. Alterations in heat-induced radiosensitization accompanied by nuclear structure alterations in Chinese hamster cells. Int J Hyperthermia. 2006; 22:43–60. [PubMed: 16423752]

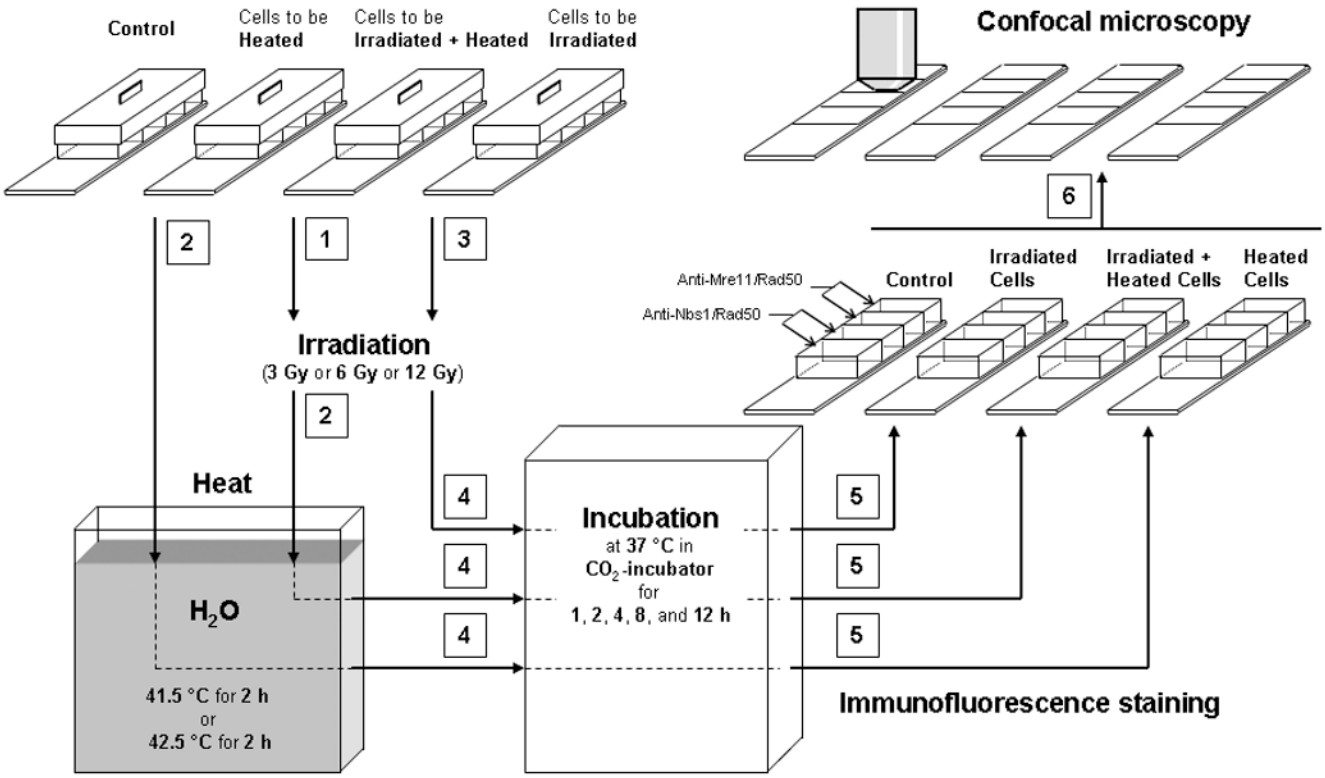

Figure 1.

Schematic representation of the sequence of procedures (sequence indicated by numbers) used to treat cells (irradiation, hyperthermia, irradiation + hyperthermia) and prepare them for analysis. Control (unheated, unirradiated) cells were kept in CO_2-incubator at 37 °C, while heating of cells (unirradiated and irradiated) was done in a water bath for 2 h at 41.5°C or 42.5°C.

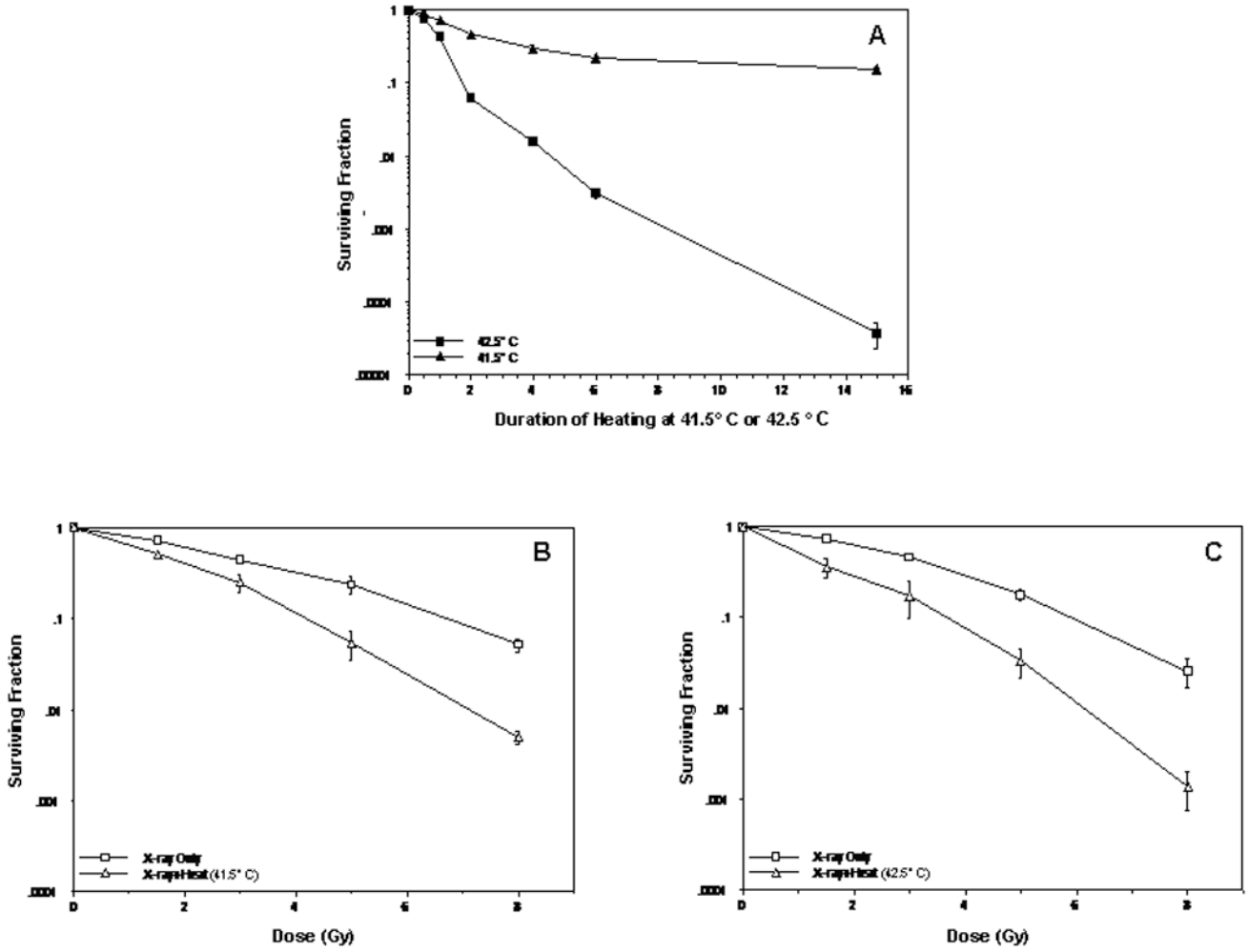

Figure 2.

Effect of 41.5°C or 42.5°C thermal treatments on unirradiated or irradiated human U-1 melanoma cells. (**A**) Clonogenic survival of cells after heating for 0.5, 1, 2, 4, 6, or 15 h at 41.5° C or 42.5° C. (B) Comparison of cell survival after irradiation with various doses of X-rays (0–8 Gy) and thermal treatment at 41.5°C for 2 h or at 42.5°C for 2 h (**C**). Surviving fractions of cells that were heated for 2 h at 41.5°C or 42.5°C (shown in panel **A**) were normalized to the surviving fraction of unheated, unirradiated cells (shown in panels **B** and **C**). Standard error of the mean for 2-3 experiments is denoted by error bars.

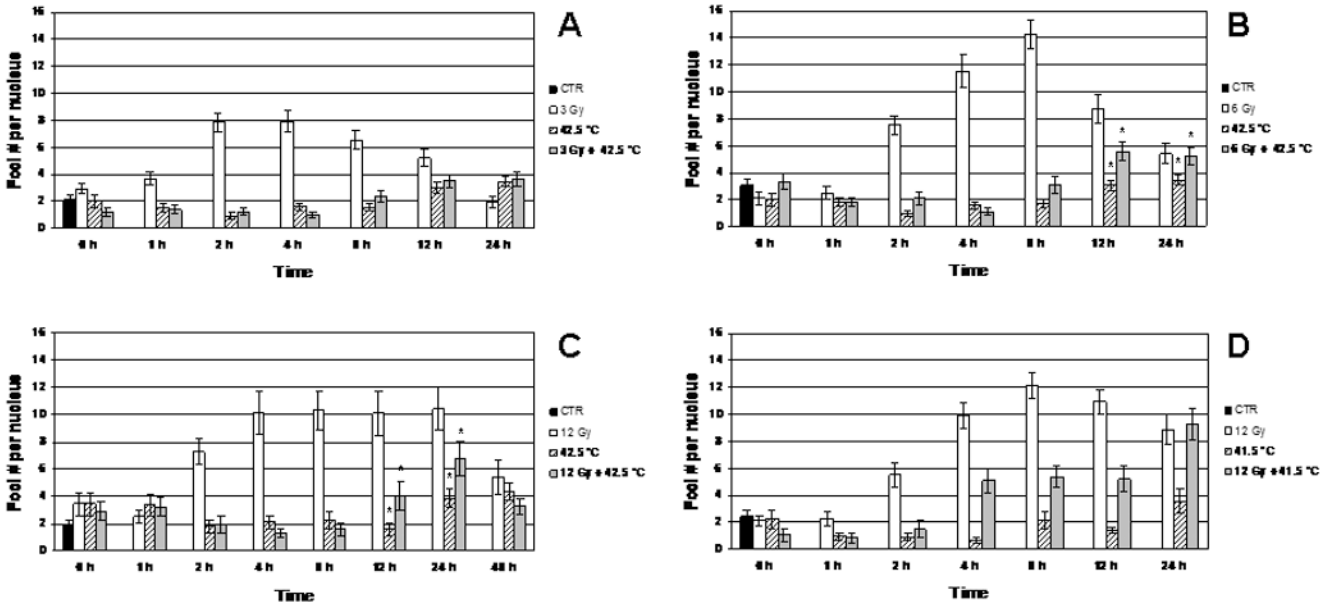

Figure 3.

A: Dynamics of Mre11/Rad50 focus formation in the nuclei of unheated 3 Gy-irradiated, 42.5°C-heated unirradiated, and 42.5°C-heated 3 Gy-irradiated cells (four independent experiments). **B**: Dynamics of Mre11/Rad50 focus formation in the nuclei of unheated 6 Gy-irradiated, 42.5°C-heated unirradiated, and 42.5°C-heated 6 Gy-irradiated cells (four independent experiments). **C**: Dynamics of Mre11/Rad50 focus formation in the nuclei of unheated 12 Gy-irradiated, 42.5°C-heated unirradiated, and 42.5°C-heated 12 Gy-irradiated cells (three independent experiments). **D**: Dynamics of Mre11/Rad50 focus formation in the nuclei of unheated 12 Gy-irradiated, 41.5°C-heated unirradiated, and 41.5°C-heated 12 Gy-irradiated cells (three independent experiments). Vertical axis shows the average number of foci per nucleus (*F*). Horizontal axis shows the post-treatment time at 37° C, in hours. Note that at 0 h post-treatment, *F* values for heated, irradiated cells and for cells that were only irradiated or heated (**A**, **B**, **C**, **D**) insignificantly differ from *F* values for control cells ($P > 0.05$). Asterisks (∗) show significant differences ($P < 0.05$) in F values between 42.5°C-heated unirradiated cells and 42.5°C-heated cells irradiated with 6 Gy or 12 Gy at 12 and 24 h post-treatment (**B**, **C**). Data presented are the mean ± standard error of the mean.

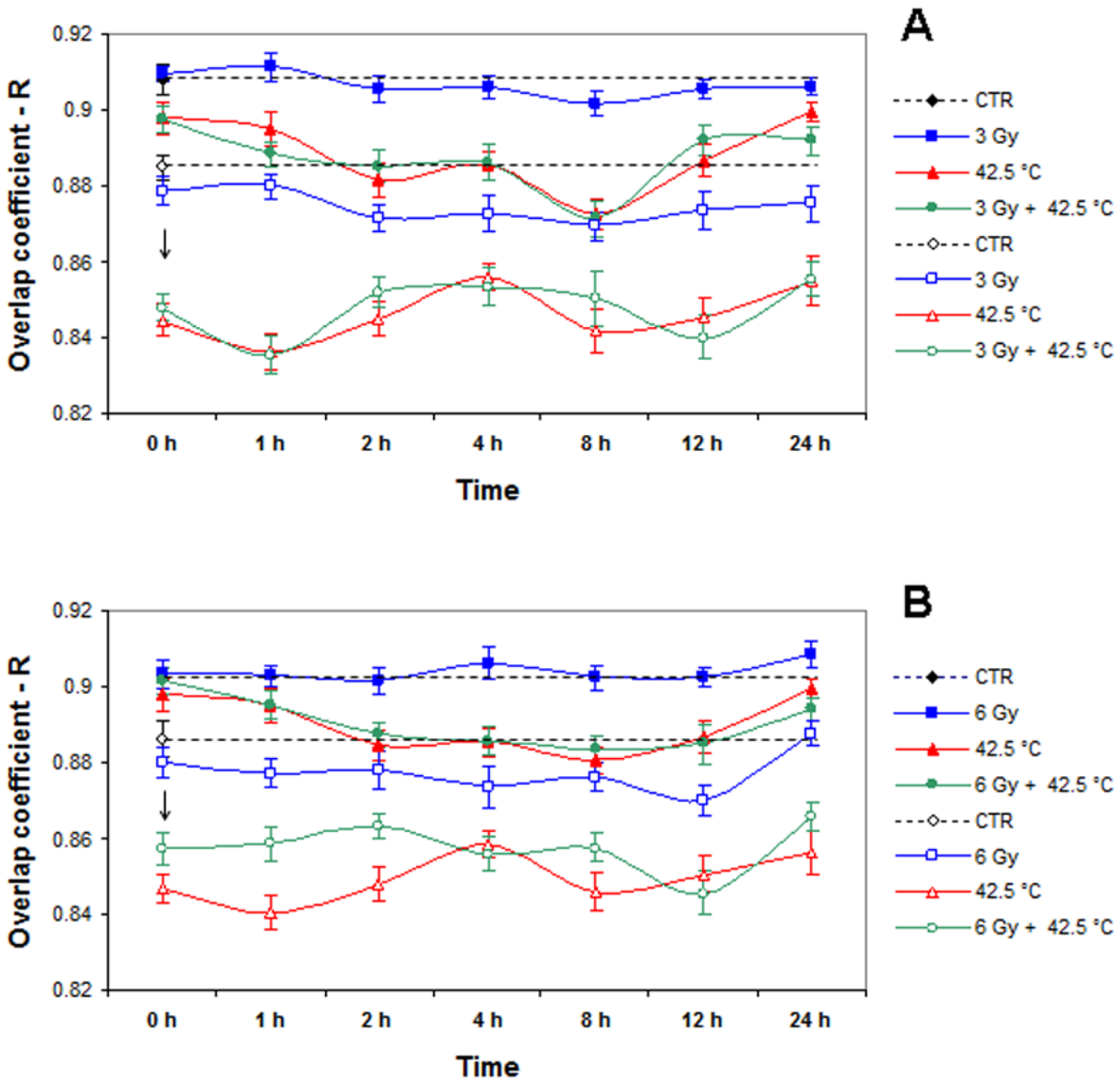

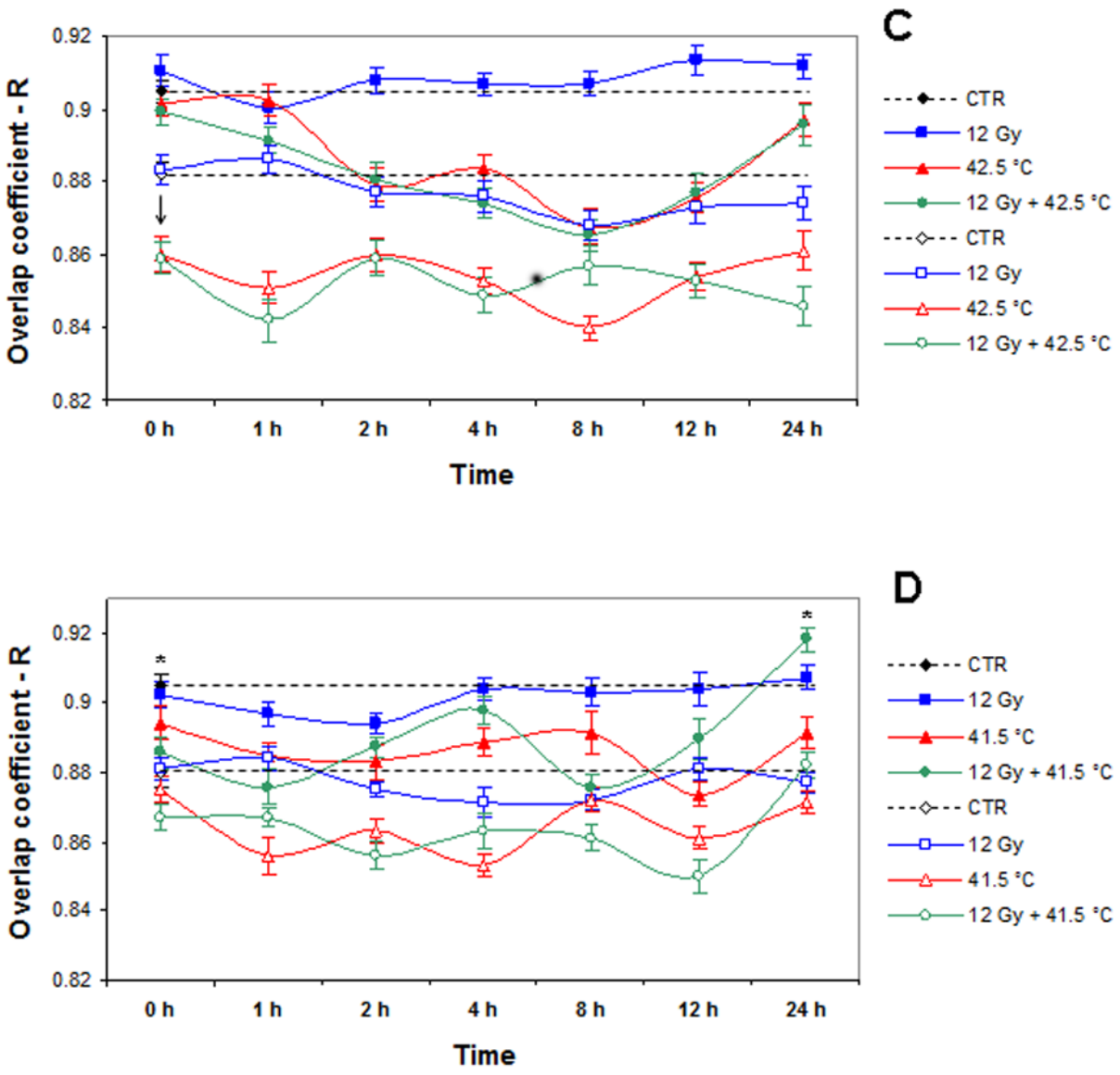

Figure 4.

A: Dynamics of changes in Mre11/Rad50 or Nbs1/Rad50 co-localization in unheated 3 Gy-irradiated, 42.5°C-heated unirradiated, and 42.5°C-heated 3 Gy-irradiated cells (four independent experiments). **B**: Dynamics of changes in Mre11/Rad50 or Nbs1/Rad50 co-localization in unheated 6 Gy-irradiated, 42.5°C-heated unirradiated, and 42.5°C-heated 6 Gy-irradiated cells (four independent experiments). **C**: Dynamics of changes in Mre11/Rad50 or Nbs1/Rad50 co-localization in unheated 12 Gy-irradiated, 42.5°C-heated unirradiated, and 42.5°C-heated 12 Gy-irradiated cells (three independent experiments). **D**: Dynamics of changes in Mre11/Rad50 or Nbs1/Rad50 co-localization in unheated 12 Gy-irradiated, 41.5°C-heated unirradiated, and 41.5°C-heated 12 Gy-irradiated cells (three independent experiments). Closed symbols show the results for Mre11/Rad50 co-localization. Open symbols show the results for Nbs1/Rad50 co-localization. Vertical axis shows the overlap coefficient according to Manders (*R*). Horizontal axis shows the post-treatment time at 37° C, in hours. For Mre11/Rad50 co-localization, at 0 h post-treatment, except 41.5°C-heated 12 Gy-irradiated cells (**D**), all other variously treated cells (**A**, **B**, **C**,

D) showed insignificant fluctuations in *R* values compared to *R* values of control cells ($P > 0.05$). For Nbs1/Rad50 co-localization, at 0 h post-treatment, except 41.5°C-heated unirradiated cells (**D**), all other variously treated cells (**A**, **B**, **C**, **D**) showed a significant drop in *R* values compared to *R* values exhibited by control cells ($P < 0.05$). Asterisks (∗) show a significant difference ($P < 0.05$) in R values between control cells and 41.5°C-heated 12 Gy-irradiated cells at 24 h post-treatment (**D**). Data presented are the mean ± standard error of the mean.

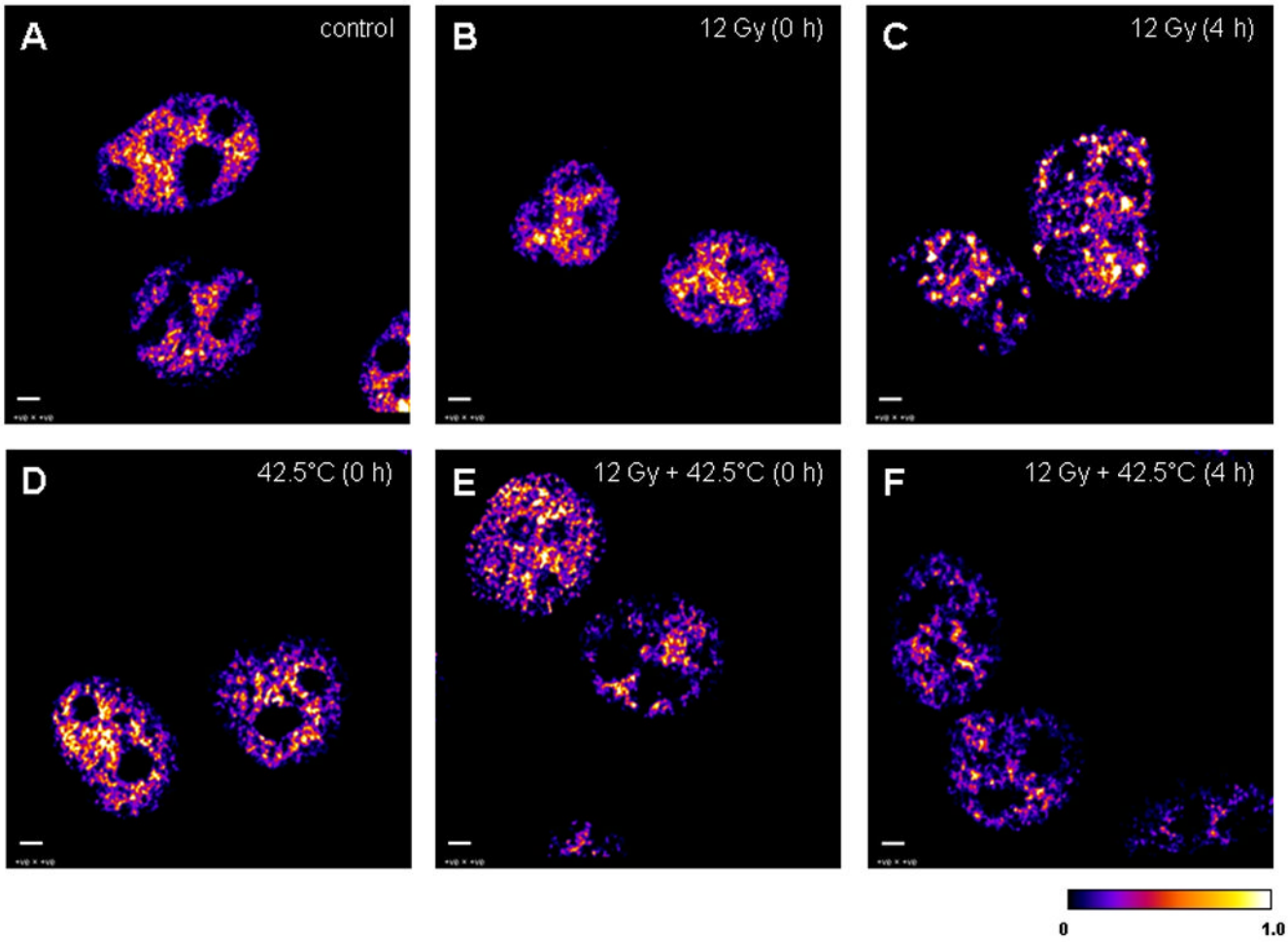

Figure 5.

The 32-bit middle plane images of positive PDM values (that represent the best correlated pixels) derived from image correlation analysis between stained Mre11 (green) and Rad50 (red) in the nuclei of unheated unirradiated (control) cells and unheated 12 Gy-irradiated, 42.5°C-heated unirradiated, and 42.5°C-heated 12 Gy-irradiated at 0 and 4 h post-treatment. **A**: the nuclei of unheated unirradiated control cells (denoted as “control”). **B**: the nuclei of unheated 12 Gy-irradiated cells at 0 h post-irradiation (denoted as “12 Gy (0 h)”). **C**: the nuclei of unheated 12 Gy-irradiated cells at 4 h post-irradiation (denoted as “12 Gy (4 h)”). **D**: the nuclei of 42.5°C-heated unirradiated cells at 0 h post-treatment (denoted as “42.5°C (0 h)”). **E**: the nuclei of 42.5°C-heated 12 Gy-irradiated cells at 0 h post-treatment (denoted as “12 Gy + 42.5°C (0 h)”). **F**: the nuclei of 42.5°C-heated 12 Gy-irradiated cells at 4 h post-treatment (denoted as “12 Gy + 42.5°C (4 h)”). A similar pattern of Mre11/Rad50 co-localization in the nuclei of control (**A**) and unheated 12 Gy-irradiated cells at 0 h post-irradiation (**B**) was observed, probably because cells were kept on ice during irradiation. *Calibration bar shows the quantitative distribution of co-localized proteins.* Scale bars = 3 μm.

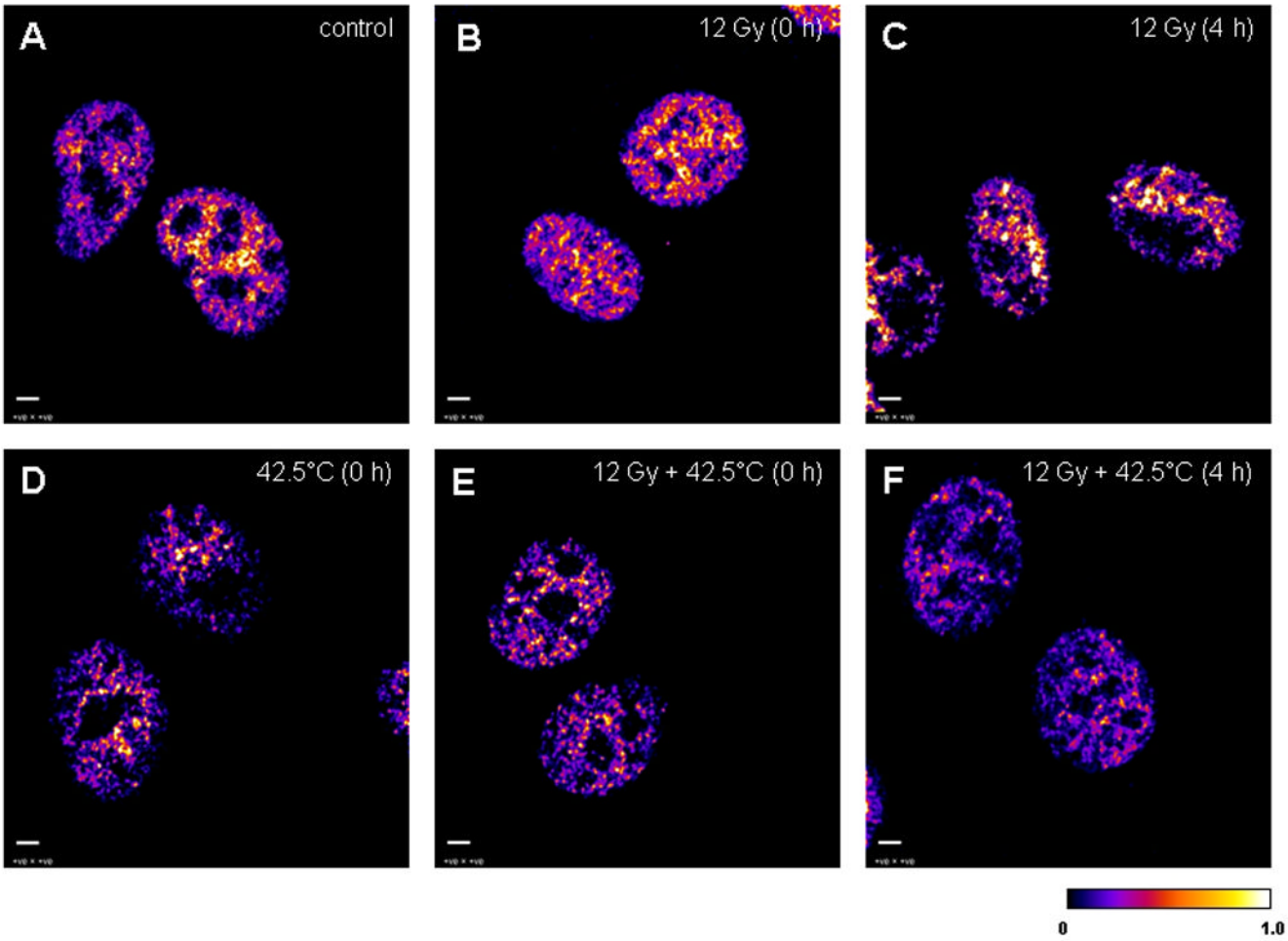

Figure 6.

The 32-bit middle plane images of positive PDM values (that represent the best correlated pixels) derived from image correlation analysis between stained Nbs1 (green) and Rad50 (red) in the nuclei of unheated unirradiated (control) cells and unheated 12 Gy-irradiated, 42.5°C-heated unirradiated, and 42.5°C-heated 12 Gy-irradiated at 0 h and 4 h post-treatment. **A**: the nuclei of unheated unirradiated control cells (denoted as “control”). **B**: the nuclei of unheated 12 Gy-irradiated cells at 0 h post-irradiation (denoted as “12 Gy (0 h)”). **C**: the nuclei of unheated 12 Gy-irradiated cells at 4 h post-irradiation (denoted as “12 Gy (4 h)”). **D**: the nuclei of 42.5°C-heated unirradiated cells at 0 h post-treatment (denoted as “42.5°C (0 h)”). **E**: the nuclei of 42.5°C-heated 12 Gy-irradiated cells at 0 h post-treatment (denoted as “12 Gy + 42.5°C (0 h)”). **F**: the nuclei of 42.5°C-heated 12 Gy-irradiated cells at 4 h post-treatment (denoted as “12 Gy + 42.5°C (4 h)”). A similar pattern of Nbs1/Rad50 co-localization in the nuclei of control (**A**) and unheated 12 Gy-irradiated cells at 0 h post-irradiation (**B**) was observed probably because cells were kept on ice during irradiation. *Calibration bar shows the quantitative distribution of co-localized proteins.* Scale bars = 3 μm.

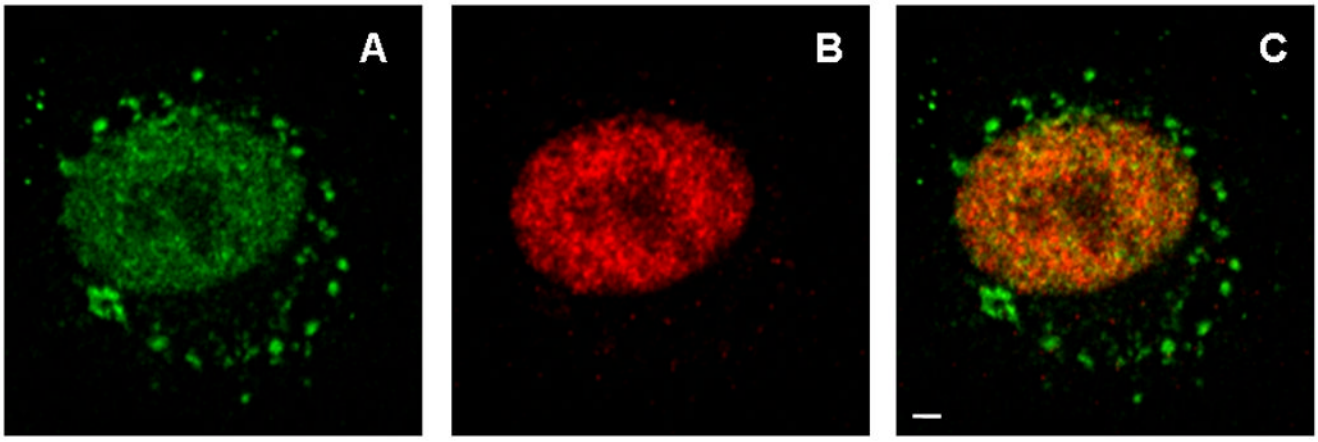

Figure 7.
Mid-plane confocal images of Nbs1 (**A**), Rad50 (**B**), and merged Nbs1 and Rad50 (**C**) immunofluorescence in a representative nucleus of one of the 42.5°C-heated unirradiated cells at 0 h post-treatment. A significant portion of Nbs1 is seen in the cytoplasm, perhaps representing aggregates of Nbs1 molecules or aggregates of Nbs1 with other molecules. Scale bar = 3 μm.

Table 1

The total numbers of nuclei of variously treated cells, in which Mre11/Rad50 co-localization was analyzed.

Time post-treatment (h)	**Control**	**3 Gy**	**42.5°C**	**3 Gy + 42.5°C**
0	69	43	61	41
1		41	62	45
2		45	60	43
4		48	60	42
8		44	62	44
12		42	60	42
24		56	62	45
Time post-treatment (h)	Control	6 Gy	42.5°C	6 Gy + 42.5°C
0	54	50	61	44
1		49	62	45
2		50	58	43
4		48	60	31
8		45	52	41
12		43	60	43
24		43	62	42
Time post-treatment (h)	Control	12 Gy	42.5°C	12 Gy + 42.5°C
0	53	37	36	40
1		40	37	35
2		62	44	43
4		50	41	42
8		44	40	44
12		32	35	36
24		39	39	39
Time post-treatment (h)	Control	12 Gy	41.5°C	12 Gy + 41.5°C
0	34	28	31	31
1		32	30	33
2		30	32	31
4		32	30	31
8		32	30	33
12		29	30	32
24		30	30	30

Table 2

The total numbers of nuclei of variously treated cells, in which Nbs1/Rad50 co-localization was analyzed.

Time post-treatment (h)	**Control**	**3 Gy**	**42.5°C**	**3 Gy + 42.5°C**
0	59	45	60	43
1		46	65	43
2		44	60	43
4		43	51	42
8		43	53	45
12		45	60	42
24		44	62	40
Time post-treatment (h)	Control	6 Gy	42.5°C	6 Gy + 42.5°C
0	41	44	79	42
1		47	81	42
2		46	75	40
4		39	68	43
8		42	69	44
12		41	76	43
24		42	74	40
Time post-treatment (h)	Control	12 Gy	42.5°C	12 Gy + 42.5°C
0	58	52	53	52
1		53	52	53
2		52	53	52
4		53	52	53
8		54	54	51
12		53	50	51
24		56	51	54
Time post-treatment (h)	Control	12 Gy	41.5°C	12 Gy + 41.5°C
0	47	31	31	30
1		30	31	30
2		34	30	32
4		30	30	30
8		32	30	30
12		32	30	30
24		30	30	30

Table 3

The total numbers of nuclei of variously treated cells, in which Mre11/Rad50 foci were quantified.

Time post-treatment (h)	**Control**	**3 Gy**	**42.5°C**	**3 Gy + 42.5°C**
0	69	42	61	37
1		43	62	45
2		43	60	43
4		49	60	42
8		44	62	43
12		42	60	42
24		56	62	45
Time post-treatment (h)	Control	6 Gy	42.5°C	6 Gy + 42.5°C
0	59	50	61	44
1		49	63	45
2		50	58	43
4		48	60	31
8		45	52	42
12		43	60	43
24		43	62	42
Time post-treatment (h)	Control	12 Gy	42.5°C	12 Gy + 42.5°C
0	51	37	36	40
1		42	37	35
2		62	44	43
4		50	41	42
8		44	41	44
12		32	35	36
24		39	39	38
48		36	38	40
Time post-treatment (h)	Control	12 Gy	41.5°C	12 Gy + 41.5°C
0	34	28	31	31
1		32	30	33
2		32	32	31
4		32	30	31
8		32	30	33
12		29	30	32
24		30	30	30